

A mixed-cation lead mixed-halide perovskite absorber for tandem solar cells

Authors: David P. McMeekin,¹ Golnaz Sadoughi,¹ Waqaas Rehman,¹ Giles E. Eperon,¹ Michael Saliba,¹ Maximilian T. Hörantner,¹ Amir Haghghirad,¹ Nobuya Sakai,¹ Lars Korte,² Bernd Rech,² Michael B. Johnston,¹ Laura M. Herz,¹ Henry J. Snaith^{1*}

Affiliations:

¹ Clarendon Laboratory, University of Oxford, Parks Road, Oxford OX1 3PU, UK

² Helmholtz-Zentrum Berlin für Materialien und Energie, Institute for Silicon Photovoltaics, Kekuléstr. 5, 12489 Berlin, Germany

*Corresponding author E-mail: henry.snaith@physics.ox.ac.uk

Abstract: Metal halide perovskite photovoltaic cells could potentially boost the efficiency of commercial silicon photovoltaic modules from ~ 20 toward 30% when used in tandem architectures. An optimum perovskite cell optical band gap of ~1.75 electron volts (eV), can be achieved by varying halide composition but to date, such materials have had poor photostability and thermal stability. Here, we present a highly crystalline and compositionally photostable material, $[\text{HC}(\text{NH}_2)_2]_{0.83}\text{Cs}_{0.17}\text{Pb}(\text{I}_{0.6}\text{Br}_{0.4})_3$ with an optical band gap of ~1.74eV, and fabricate perovskite cells which reach open-circuit voltages of 1.2 V and power conversion efficiency of over 17% on small areas and 14.7% on 0.715 cm² cells. By combining with a 19% efficient silicon cell we demonstrate the feasibility of achieving > 25% efficient four-terminal tandem cells.

One concept for improving the efficiency of photovoltaics (PVs) is to create a “tandem junction,” for example, by placing a wide band gap “top cell” above a silicon “bottom cell.” This approach could realistically increase the efficiency of the Si cell from 25.6% to beyond 30% (1, 2). Given the crystalline silicon (c-Si) band gap of 1.1 eV, the top cell material requires a band gap of ~1.75 eV, in order to current-match both junctions (3). However, suitable wide-band-gap top-cell materials for Si or thin film technologies that offer stability, high performance, and low cost have been lacking. In recent years, metal halide perovskite-based PVs have gained attention because of their high power conversion efficiencies (PCE) and low processing cost (4–11). An attractive feature of this material is the ability to tune its band gap from 1.48 to 2.3 eV (12, 13), implying that we could potentially fabricate an ideal material for tandem cell applications.

Perovskite-based PVs are generally fabricated with organic-inorganic trihalide perovskites with the formulation ABX_3 , where A is the methylammonium (CH_3NH_3) (MA) or formamidinium ($\text{HC}(\text{NH}_2)_2$) (FA) cation, B is commonly lead (Pb), while X is a halide (Cl, Br, and I). Although these perovskite structures offer high power conversion efficiencies (PCE), reaching > 20% PCE with band gaps of around 1.5 eV (14), fundamental issues have been discovered when attempting to tune their band gaps to the optimum 1.7 to 1.8 eV range. In the case of $\text{MAPb}(\text{I}_{(1-x)}\text{Br}_x)_3$, Hoke *et al.* reported that light-soaking induces a halide segregation within the perovskite (15). The formation of iodide-rich domains with lower band gap result in an increase in sub-gap absorption and a red-shift of photoluminescence (PL). The lower band gap regions limit the voltage attainable with such a material, so this band gap “photoinstability” limits the use of $\text{MAPb}(\text{I}_{(1-x)}\text{Br}_x)_3$ in tandem devices (15). In addition, when considering real-world applications, MAPbI_3 is inherently thermally unstable at 85°C, even in an inert atmosphere (international regulations require a commercial PV product to withstand this temperature) (16).

Concerning the more thermally stable FAPbX₃ perovskite, an increase in optical band gap has not resulted in an expected increase in V_{OC} (13). Furthermore, as iodide is substituted with bromide, a crystal phase transition occurs from a trigonal to a cubic structure; in compositions near the transition, the material is unable to crystallize, resulting in an apparently “amorphous” phase with high levels of energetic disorder and unexpectedly low absorption. These compositions additionally have much lower charge-carrier mobilities in the range of $1 \text{ cm}^2\text{V}^{-1}\text{s}^{-1}$, in comparison to $> 20 \text{ cm}^2\text{V}^{-1}\text{s}^{-1}$, in the neat iodide perovskite (17). For tandem applications, these problems arise at the Br composition needed to form the desired top-cell band gap of ~ 1.7 to 1.8 eV .

Nevertheless, perovskite/Si tandem PVs have already been reported in a four-terminal (18, 19) and two-terminal architectures (20). However, their reported efficiencies have yet to surpass the optimized single-junction efficiencies, in part because of non-ideal absorber band gaps. It is possible to form a lower band gap triiodide perovskite material and current-match the top and bottom junctions in a monolithic architecture by simply reducing the thickness of the top cell. However, this method results in a non-ideal efficiency.

Herein, we address the issues of forming a photostable FA based perovskite with the ideal band gap for tandem PVs. We partially substitute the formamidinium cation with Cs and make the remarkable observation that the phase instability region is entirely eliminated in the iodide to bromide compositional range, delivering complete tunability of the band gap around 1.75 eV . We fabricate planar heterojunction perovskite PVs, demonstrating PCE of $> 17\%$ and stabilized power output (SPO) of 16% . To demonstrate the potential impact of this new perovskite material in tandem solar cells, we create a semi-transparent perovskite device, and measure the performance of a silicon PV after “filtering” the sunlight through the perovskite top cell. The Si cells delivered an efficiency boost of 7.3% , indicating the feasibility for achieving $> 25\%$ efficient perovskite/Si tandem cells.

The A-site cations that could be used with lead halides to form suitable perovskites for PVs are Cs, MA, and FA. CsPbI₃ does form a “black phase” perovskite with a band gap of 1.73 eV , however, this appropriate phase is only stable at temperatures above 200° to 300°C and the most stable phase at room temperature is a non-perovskite orthorhombic “yellow” phase. MA based perovskites are thermally unstable and suffer from halide segregation instabilities, and are thus likely to be unsuitable (16). FA based perovskites are the most likely to deliver the best balance between structural and thermal stability (13, 21–25). However, in Fig. 1A, we show photographs of a series of FAPb(I_(1-x)Br_x)₃ films; we observe a “yellowing” of the films for compositions of x between 0.3 and 0.6 , consistent with the previously reported phase instability caused by a transition from a trigonal ($x < 0.3$) to cubic ($x > 0.5$) structures (13).

We have previously observed that the band gap changes from 1.48 eV for FAPbI₃ to 1.73 eV for CsPbI₃ (13). Recently it has been shown that mixing Cs with FA or MA, results in a slight widening of the band gap (26, 27). We considered here the possibility that if we partially substitute FA for Cs, we could push this region of structural instability in the Br to I phase-space to higher energies, and thus potentially achieve a structurally stable mixed halide perovskite with a band gap of 1.75 eV . In Fig 1B, we show photographs of thin films fabricated from mixed-cation lead mixed-halide FA_{0.83}Cs_{0.17}Pb(I_(1-x)Br_x)₃ compositions. Unexpectedly, we do not simply shift the region of structural instability to higher energy, but we observe a continuous series of dark films throughout this entire compositional range. To confirm these observations, we also perform ultraviolet-visible absorption measurements. We obtained a sharp optical band edge for all compositions of the FA_{0.83}Cs_{0.17}Pb(I_(1-x)Br_x)₃.

x)Br $_x$) $_3$ material (Fig. 1, C and D), in contrast to FAPb(I $_{1-x}$)Br $_x$) $_3$, which shows weak absorption in the intermediate range.

In order to understand the impact of adding Cs upon the crystallization of the perovskite, we performed x-ray diffraction (XRD) on the series of films covering the I to Br compositional range. In Fig. 1E, we show the XRD patterns for FAPb(I $_{1-x}$)Br $_x$) $_3$, zoomed in to the peak around $2\theta \sim 14^\circ$ [the complete diffraction pattern is shown in Fig. S1, along with more details on fitting this data (28)]. Quite remarkably, for the FA $_{0.83}$ Cs $_{0.17}$ Pb(I $_{1-x}$)Br $_x$) $_3$, the material is in a single phase throughout the entire composition range. The monotonic shift of the (100) reflection which we observed from $2\theta \sim 14.2^\circ$ to 14.9° , is consistent with a cubic lattice constant shift from 6.306 to 5.955Å as the material incorporates a larger fraction of the smaller halide, Br [in Fig. S2, we show the complete diffraction pattern (28)]. Thus, for the FA $_{0.83}$ Cs $_{0.17}$ Pb(I $_{1-x}$)Br $_x$) $_3$ perovskite, we have removed the structural phase transition and instability over the entire compositional range [in Fig. S3 to S5 we show details of varying the Cs concentration and the Br to I concentration (28)]. Quite remarkably over the entire Br to I range, and for a large fraction of the Cs-FA range, the variation in lattice constant, composition and optical band gap precisely follow Vegard's law [Fig. S6 (28)], so we have total flexibility and predictability in tuning of the composition and its impact upon the band gap. For the results that follow below, we will use the precise composition FA $_{0.83}$ Cs $_{0.17}$ Pb(I $_{0.6}$ Br $_{0.4}$) $_3$, which has an optical a band gap of 1.74eV as determined by a Tauc plot [Fig. S7 (28)].

Photoinduced halide segregation has been reported in methylammonium lead mixed halide perovskites (15). A red-shift in PL upon light illumination, for intensities ranging from 10 to 100 mW cm $^{-2}$ occurs, with the shift to lower energies resulting from the formation of iodine-rich domains that have lower band gaps. This limits the achievable open-circuit voltage of the solar cell device by introducing a large degree of electronic disorder. In Fig. 2, we show the PL from films of MAPb(I $_{0.6}$ Br $_{0.4}$) $_3$ perovskite and the mixed cation mixed halide material FA $_{0.83}$ Cs $_{0.17}$ Pb(I $_{0.6}$ Br $_{0.4}$) $_3$, immediately after prolonged periods of light exposure, using a power density of ~ 3 mW cm $^{-2}$ and a wavelength of 550 nm as excitation source. We confirm the results observed by Hoke *et al.*, where we see a time-dependent red-shift in PL for the MAPb(I $_{0.6}$ Br $_{0.4}$) $_3$ film, which exhibits a 130 meV PL red-shift after only 1 hour of illumination. We also show the time evolution of the PL from MAPb(I $_{0.8}$ Br $_{0.2}$) $_3$, a composition previously reported in devices (29), which shifts from 1.72eV to 1.69eV [Fig. S8 (28)]. In contrast, although we see a rise in PL intensity, we observe no significant red-shift in PL emission for the FA $_{0.83}$ Cs $_{0.17}$ Pb(I $_{0.6}$ Br $_{0.4}$) $_3$ precursor composition after 1 hour of identical light illumination (which we show in Fig. 2B). Furthermore, we exposed a similar FA $_{0.83}$ Cs $_{0.17}$ Pb(I $_{0.6}$ Br $_{0.4}$) $_3$ film to monochromatic irradiance of much higher 5 Wcm $^{-2}$ irradiance, and observed no red shift after 240 s of illumination [Fig. S9,(28)]. Under these identical conditions, we did observe a red shift in the PL for the single cation FAPb(I $_{0.6}$ Br $_{0.4}$) $_3$ perovskite, as we have previously reported (17). In addition, under thermal stressing at 130 °C, we observe that optical band gap and the crystal lattice of FA $_{0.83}$ Cs $_{0.17}$ Pb (I $_{0.6}$ Br $_{0.4}$) is stable, in contrast to MAPb(I $_{0.6}$ Br $_{0.4}$) $_3$ [Fig. S10].

Beyond halide segregation, a further deleterious observation previously made for mixed halide perovskites has been that the energetic disorder in the material is greatly increased in comparison to the neat iodide perovskites. The ultimate open-circuit voltage a solar cell material can generate is intimately linked to the steepness of the absorption onset just below the band edge, which can be quantified by the Urbach energy (E_u) (30, 31). This E_u reported by De Wolf *et al.* and Sadhanala *et al.* for MAPbI $_3$ was 15 meV (31), where small values of E_u indicate low levels of electronic disorder. In contrast, the E_u for MAPb(I $_{0.6}$ Br $_{0.4}$) $_3$ perovskite increases to 49.5 meV (32). We determined E_u by performing Fourier-transform photocurrent spectroscopy (FTPS) on complete planar heterojunction

solar cells (details of the solar cells will be discussed below) and in Fig. 2C we show the semi-log plot of external quantum efficiency (EQE) absorption edge of a device fabricated with the optimized precursor solution and annealing procedure. We calculated an E_u of 16.5 meV, near the values reported for the neat iodide perovskites.

In order to further assess the electronic quantity of $\text{FA}_{0.83}\text{Cs}_{0.17}\text{Pb}(\text{I}_{0.6}\text{Br}_{0.4})_3$ we have performed optical-pump terahertz-probe (OPTP) spectroscopy, which is a noncontact method of probing the photoinduced conductivity and effective charge carrier mobility in the material. In Fig. 2D, we show the fluence-dependence of the OPTP transients, which exhibit accelerated decay dynamics at higher initial photoinjected charge-carrier densities, as the result of enhanced contributions from bimolecular and Auger recombination. We may extract the rate constants associated with different recombination mechanisms by global fits to these transient of the solutions to the rate equation:

$$\frac{dn(t)}{dt} = -k_3n^3 - k_2n^2 - k_1n \quad (1)$$

We find that $\text{FA}_{0.83}\text{Cs}_{0.17}\text{Pb}(\text{I}_{0.6}\text{Br}_{0.4})_3$ exhibits an excellent charge-carrier mobility of $21 \text{ cm}^2\text{V}^{-1}\text{s}^{-1}$. For comparison, the corresponding neat-FA perovskite $\text{FAPb}(\text{I}_{0.6}\text{Br}_{0.4})_3$ only sustains charge-carrier mobilities $<1 \text{ cm}^2\text{V}^{-1}\text{s}^{-1}$ that are related to the amorphous and energetically disordered nature of these materials (17). Conversely, $\text{FA}_{0.83}\text{Cs}_{0.17}\text{Pb}(\text{I}_{0.6}\text{Br}_{0.4})_3$ displays a mobility value intermediate to those we have previously determined (17) for FAPbI_3 ($27 \text{ cm}^2\text{V}^{-1}\text{s}^{-1}$) and FAPbBr_3 ($14 \text{ cm}^2\text{V}^{-1}\text{s}^{-1}$) suggesting that it is no longer limited by structural disorder.

We find that $\text{FA}_{0.83}\text{Cs}_{0.17}\text{Pb}(\text{I}_{0.6}\text{Br}_{0.4})_3$ exhibits an excellent charge-carrier mobility of $21 \text{ cm}^2\text{V}^{-1}\text{s}^{-1}$. For comparison, the corresponding neat-FA perovskite $\text{FAPb}(\text{I}_{0.6}\text{Br}_{0.4})_3$ only sustains charge-carrier mobilities $<1 \text{ cm}^2\text{V}^{-1}\text{s}^{-1}$ that are related to the amorphous and energetically disordered nature of these materials (17). Conversely, $\text{FA}_{0.83}\text{Cs}_{0.17}\text{Pb}(\text{I}_{0.6}\text{Br}_{0.4})_3$ displays a mobility value intermediate to those we have previously determined (17) for FAPbI_3 ($27 \text{ cm}^2\text{V}^{-1}\text{s}^{-1}$) and FAPbBr_3 ($14 \text{ cm}^2\text{V}^{-1}\text{s}^{-1}$) suggesting that it is no longer limited by structural disorder.

We further assesses the potential of $\text{FA}_{0.83}\text{Cs}_{0.17}\text{Pb}(\text{I}_{0.6}\text{Br}_{0.4})_3$ for incorporation into planar heterojunction PV architectures by deriving the charge-carrier diffusion length $L=(\mu k_B T/(eR))^{0.5}$ as function of the charge-carrier density n , where $R=k_1+nk_2+n^2k_3$ is the total recombination rate, k_B the Boltzmann constant, T temperature and e the elementary charge. In Fig. 2E, we show that for charge-carrier densities typical under solar illumination ($n\sim 10^{15}\text{cm}^{-3}$) a value of $L\sim 2.9 \mu\text{m}$ is reached, comparable to values reported for high-quality thin films of neat lead iodide perovskites (17, 33). The high charge-carrier mobility and slow recombination kinetics, and long charge carrier diffusion length imply that this mixed cation, mixed halide perovskite should be just as effective as a high-quality solar cell absorber material as the neat halide perovskite FAPbI_3 .

We fabricated a series of planar heterojunction solar cells to assess the overall solar cell performance [we describe in more detail and show data for solar cells fabricated with a range of compositional and processing parameters in Fig. S11 (28)]. We show the device architecture in Fig. 3A, which is composed of a SnO_2 /phenyl- C_{60} -butyric acid methyl ester (PC₆₀BM) electron-selective layer, a solid $\text{FA}_{0.83}\text{Cs}_{0.17}\text{Pb}(\text{I}_{0.6}\text{Br}_{0.4})_3$ perovskite absorber layer, and Li-TFSI-doped spiro-OMeTAD with 4-tert-butylpyridine (TBP) additive as the hole-collection layer, capped with an Ag electrode. We measured current–voltage (I - V) characteristics of such devices under simulated air-mass (AM) 1.5 100 mW cm^{-2} sunlight, and show the I - V characteristics of one the highest performing device in Fig. 3B. It delivered a short-circuit current density of 19.4 mA cm^{-2} , a V_{OC} of 1.2 V, and a PCE of 17.1 %. By

holding the cell at a fixed maximum power point forward bias voltage of 0.95 V, we measured the power output over time reaching a stabilized efficiency of 16% (Fig. 3C). The highest JV efficiency we measured was 17.9% [Fig. S12 (28), along with a histogram of performance parameters for a large batch of devices in Fig. S13 (28)]. To demonstrate that these cells can also operate with larger area, we fabricated 0.715 cm² active layers where the cells reach a stabilized power output of > 14% [Fig. S14(28)]. In Fig 3D, we show the spectral response of the solar cell, which confirms the wider band gap of the solar cell, and also integrates over the AM1.5 solar spectrum to give 19.2 mA cm⁻², in close agreement to the measured J_{SC} .

This performance is very competitive with the best reported single junction perovskite solar cell reported so far, (30, 34), especially considering the wider band gap of our material which should result in a few percent absolute efficiency drop with respect to a 1.55eV material (35). Importantly for tandem solar cells, this 1.74 eV material appears to be capable of generating a higher V_{OC} than the 1.55 eV triiodide perovskites in planar heterojunction solar cells. Following Rau *et al.* (36), from the integration of the EQE over the black body radiation spectrum, we estimate the maximum attainable V_{OC} for our FA_{0.83}Cs_{0.17}Pb(I_{0.6}Br_{0.4})₃ device to be 1.42 V [details shown in Fig. S15], which is 100 mV higher than that estimated for MAPbI₃ devices by Tvingstedt *et al.* and Tress *et al.*(30, 34).

In order to demonstrate the potential impact of using this new perovskite composition in a tandem architecture, we fabricated semitransparent perovskite solar cells by sputter coating ITO on top of the perovskite cells, with the additional inclusion of a thin “buffer layer” of solution processed ITO nanoparticles between the spiro-OMeTAD and the ITO. The efficiency of the semi-transparent FA_{0.83}Cs_{0.17}Pb(I_{0.6}Br_{0.4})₃ solar cells is 15.1%, as determined by the I - V curve, with a stabilized power output of 12.5%. Because J_{SC} is similar to the cell with the Ag electrode, we expect that the slight drop in V_{OC} and SPO will be surmountable by better optimization of the ITO sputter deposition procedure and buffer layer. We measured a Si heterojunction (SHJ) cell, with and without a semi-transparent perovskite cell held in front of it, and determined an efficiency of 7.3% filtered, and 19.2% when uncovered. These results demonstrate the feasibility of obtaining a combined tandem solar cell efficiency ranging from 19.8%, if we combine with the stabilized power output of the semi-transparent cell, to 25.2% if we combine with the highest JV measured efficiency of the FA_{0.83}Cs_{0.17}Pb(I_{0.6}Br_{0.4})₃ cell. Considering further minor improvements in the perovskite, optical management and integration and choice of Si rear cell, it is feasible that this system could deliver up to 30% efficiency. In addition, this monotonic tunability of band gap across the visible spectrum within a single crystalline phase, will have direct impact to the color tunability and optimization of perovskites for light emitting applications.

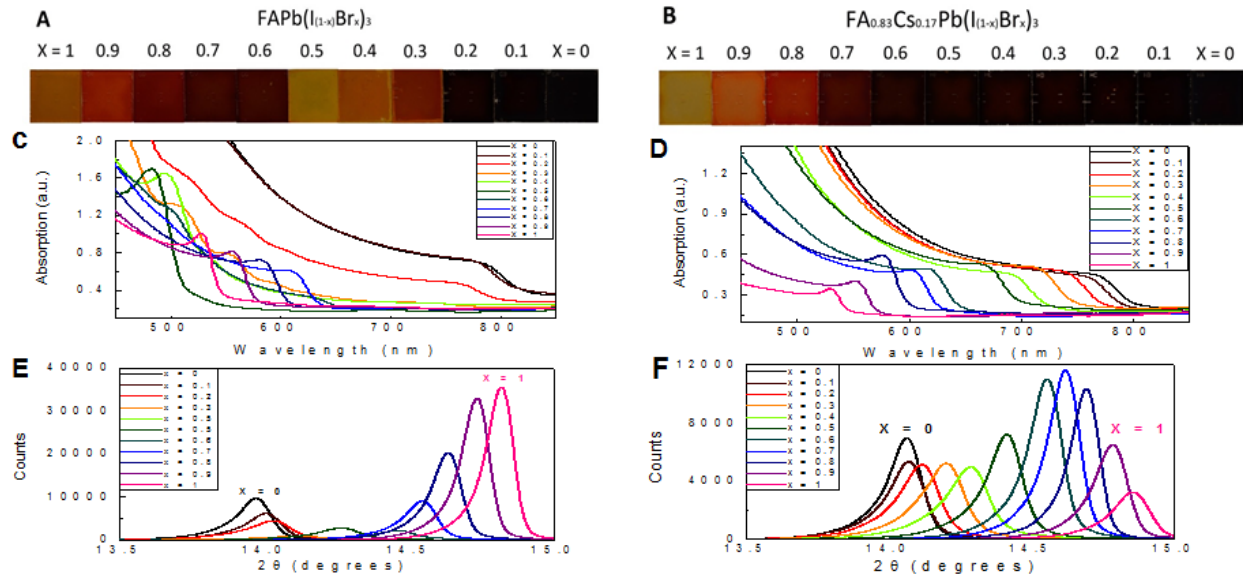


Fig. 1 Tuning the band-gap. Photographs of perovskite films with Br composition increasing from $x = 0$ to 1 for (A) $\text{FAPb}(\text{I}_{1-x}\text{Br}_x)_3$ and (B) $\text{FA}_{0.83}\text{Cs}_{0.17}\text{Pb}(\text{I}_{1-x}\text{Br}_x)_3$. (C) UV-Vis absorbance spectra of films of $\text{FAPb}(\text{I}_{1-x}\text{Br}_x)_3$ and (D) $\text{FA}_{0.83}\text{Cs}_{0.17}\text{Pb}(\text{I}_{1-x}\text{Br}_x)_3$. (E) X-ray diffraction (XRD) pattern of $\text{FAPb}(\text{I}_{1-x}\text{Br}_x)_3$ and (F) $\text{FA}_{0.83}\text{Cs}_{0.17}\text{Pb}(\text{I}_{1-x}\text{Br}_x)_3$. We note that the stated compositions are the fractional compositions of the ions in the starting solution, and the actual composition of the crystallized films may vary slightly.

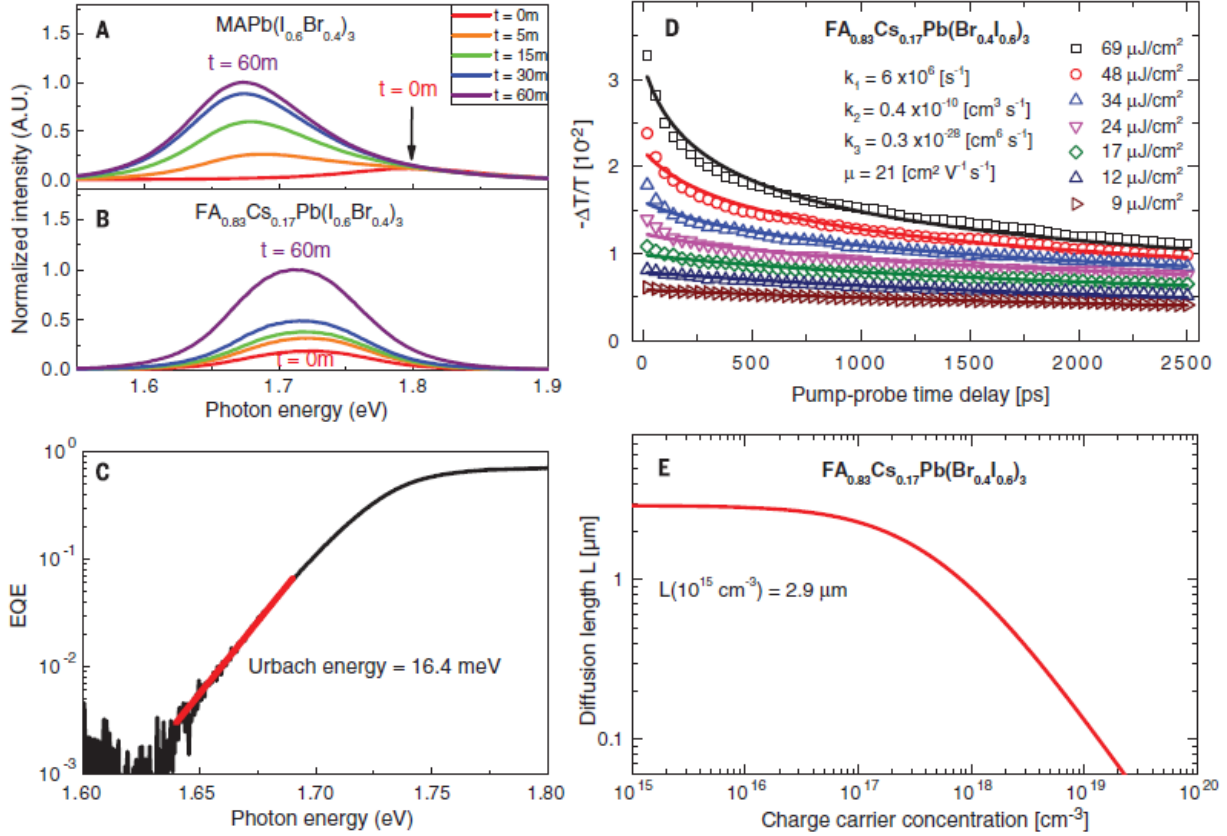


Fig. 2 Material characteristics of $\text{FA}_{0.83}\text{Cs}_{0.17}\text{Pb}(\text{I}_{0.6}\text{Br}_{0.4})_3$ perovskite material. Normalized photoluminescence (PL) measurement measured after 0, 5, 15, 30 and 60 minutes of light exposure of the (A) $\text{MAPb}(\text{I}_{0.6}\text{Br}_{0.4})_3$ and (B) $\text{FA}_{0.83}\text{Cs}_{0.17}\text{Pb}(\text{I}_{0.6}\text{Br}_{0.4})_3$ thin films. (C) Semi-log plot of external quantum efficiency (EQE) at the absorption onset for a $\text{FA}_{0.83}\text{Cs}_{0.17}\text{Pb}(\text{I}_{0.6}\text{Br}_{0.4})_3$ PV cell, measured using FTPS at short-circuit (J_{sc}). (D) OPTP transients for a $\text{FA}_{0.83}\text{Cs}_{0.17}\text{Pb}(\text{I}_{0.6}\text{Br}_{0.4})_3$ thin film, measured following excitation with a 35fs light pulse of wavelength 400nm with different fluences. (E) Charge-carrier diffusion length L as a function of charge concentration.

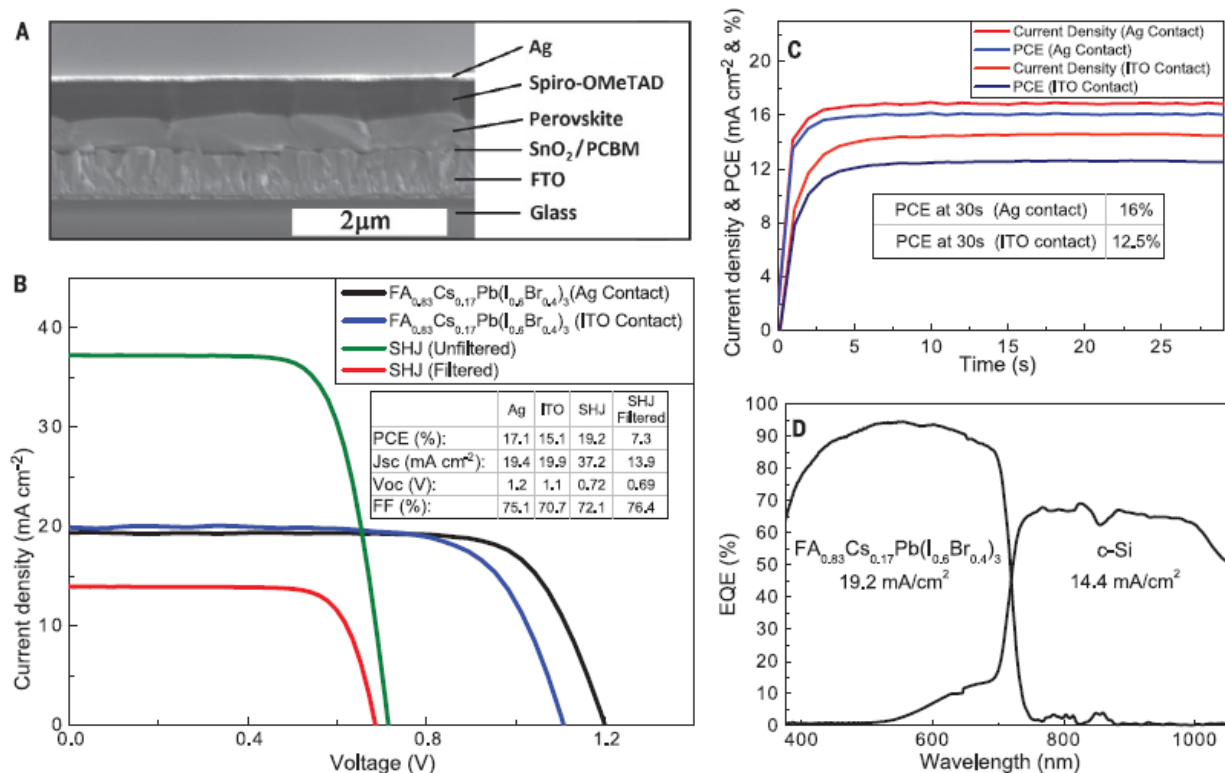


Fig. 3. Device architecture and I-V characteristics for $\text{FA}_{0.83}\text{Cs}_{0.17}\text{Pb}(\text{I}_{0.6}\text{Br}_{0.4})_3$ perovskite and Si PV cells. (A) SEM image of cross-section of a planar heterojunction solar cell (B) Forward bias to short-circuit I-V curve for the best perovskite devices fabricated, using either a Ag metal, or semi-transparent ITO top electrode, measured at 0.38V/s scan rate. We also show the current voltage curve of a silicon heterojunction (SHJ) cell, measured with direct light or with the simulated sunlight filtered through the semi-transparent perovskite solar cell (37). We note that the SHJ cells were measured at the Centre For Renewable Energy Technologies (CREST), Loughborough UK under an extremely well calibrated solar simulator. (C) Photocurrent density and power conversion efficiency measured at maximum power point for a 30s time span (D) External quantum efficiency (EQE) spectrum measured in short-circuit (J_{sc}) configuration for the highest efficiency perovskite cell and the SHJ cell measured with the incident light filtered through the semi-transparent perovskite cell.

References and Notes

1. V. Sivaram, S. D. Stranks, H. J. Snaith, Outshining Silicon. *Sci. Am.* **313**, 54–59 (2015).
2. M. A. Green, K. Emery, Y. Hishikawa, W. Warta, E. D. Dunlop, Solar cell efficiency tables (version 46). *Prog. Photovoltaics Res. Appl.* **23**, 805–812 (2015).
3. A. Shah, P. Torres, R. Tscharnner, N. Wyrsh, H. Keppner, Photovoltaic Technology: The Case for Thin-Film Solar Cells. *Science*. **285**, 692–699 (1999).
4. C. R. Kagan, Organic-Inorganic Hybrid Materials as Semiconducting Channels in Thin-Film Field-Effect Transistors. *Science*. **286**, 945–947 (1999).
5. A. Kojima, K. Teshima, Y. Shirai, T. Miyasaka, Organo Metal Halide Perovskites as Visible-Light Sensitizer for Photovoltaic Cells. *Priv. Commun.* **1**, 1 (2009).
6. M. M. Lee, J. Teuscher, T. Miyasaka, T. N. Murakami, H. J. Snaith, Efficient Hybrid Solar Cells Based on Meso-Superstructured Organometal Halide Perovskites. *Science*.

- 338, 643–647 (2012).
7. M. Liu, M. B. Johnston, H. J. Snaith, Efficient planar heterojunction perovskite solar cells by vapour deposition. *Nature*. **501**, 395–8 (2013).
 8. J. Burschka *et al.*, Sequential deposition as a route to high-performance perovskite-sensitized solar cells. *Nature*. **499**, 316–9 (2013).
 9. M. a. Green, A. Ho-Baillie, H. J. Snaith, The emergence of perovskite solar cells. *Nat. Photonics*. **8**, 506–514 (2014).
 10. N. J. Jeon *et al.*, Solvent engineering for high-performance inorganic-organic hybrid perovskite solar cells. *Nat. Mater.* **13**, 1–7 (2014).
 11. N. J. Jeon *et al.*, Compositional engineering of perovskite materials for high-performance solar cells. *Nature*. **517**, 476–480 (2015).
 12. J. H. Noh, S. H. Im, J. H. Heo, T. N. Mandal, S. Il Seok, Chemical management for colorful, efficient, and stable inorganic-organic hybrid nanostructured solar cells. *Nano Lett.* **13**, 1764–9 (2013).
 13. G. E. Eperon *et al.*, Formamidinium lead trihalide: a broadly tunable perovskite for efficient planar heterojunction solar cells. *Energy Environ. Sci.* **7**, 982 (2014).
 14. W. S. Yang *et al.*, High-performance photovoltaic perovskite layers fabricated through intramolecular exchange. *Science*. **348**, 1234–1237 (2015).
 15. E. T. Hoke *et al.*, Reversible photo-induced trap formation in mixed-halide hybrid perovskites for photovoltaics. *Chem. Sci.* **6**, 613–617 (2014).
 16. B. Conings *et al.*, *Adv. Energy Mater.*, in press, doi:10.1002/aenm.201500477.
 17. W. Rehman *et al.*, *Adv. Mater.*, in press, doi:10.1002/adma.201502969.
 18. C. D. Bailie *et al.*, Semi-transparent perovskite solar cells for tandems with silicon and CIGS. *Energy Environ. Sci.* **8**, 956–963 (2015).
 19. P. Löper *et al.*, Organic-inorganic halide perovskite/crystalline silicon four-terminal tandem solar cells. *Phys. Chem. Chem. Phys.* **17**, 1619–29 (2015).
 20. S. Albrecht *et al.*, Monolithic Perovskite/Silicon-Heterojunction Tandem Solar Cells Processed at Low Temperature. *Energy Environ. Sci.* (2015), doi:10.1039/C5EE02965A.
 21. A. Binek, F. C. Hanusch, P. Docampo, T. Bein, Stabilization of the Trigonal High Temperature Phase of Formamidinium Lead Iodide. *J. Phys. Chem. Lett.* **6**, 150316103833007 (2015).
 22. S. Pang *et al.*, NH₂CH=NH₂PbI₃: An Alternative Organolead Iodide Perovskite Sensitizer for Mesoscopic Solar Cells. *Chem. Mater.* **26**, 1485–1491 (2014).
 23. C. C. Stoumpos, C. D. Malliakas, M. G. Kanatzidis, Semiconducting tin and lead iodide perovskites with organic cations: phase transitions, high mobilities, and near-infrared photoluminescent properties. *Inorg. Chem.* **52**, 9019–38 (2013).
 24. N. Pellet *et al.*, Mixed-organic-cation perovskite photovoltaics for enhanced solar-light harvesting. *Angew. Chem. Int. Ed. Engl.* **53**, 3151–7 (2014).
 25. S. D. Stranks, H. J. Snaith, Metal-halide perovskites for photovoltaic and light-emitting devices. *Nat. Nanotechnol.* **10**, 391–402 (2015).
 26. J.-W. Lee *et al.*, *Adv. Energy Mater.*, in press, doi:10.1002/aenm.201501310.
 27. H. Choi *et al.*, Cesium-doped methylammonium lead iodide perovskite light absorber for hybrid solar cells. *Nano Energy*. **7**, 80–85 (2014).
 28. See supplementary materials on Science Online.
 29. C. Bi, Y. Yuan, Y. Fang, J. Huang, *Adv. Energy Mater.*, in press, doi:10.1002/aenm.201401616.

30. K. Tvingstedt *et al.*, Radiative efficiency of lead iodide based perovskite solar cells. *Sci. Rep.* **4**, 6071 (2014).
31. S. De Wolf *et al.*, Organometallic Halide Perovskites: Sharp Optical Absorption Edge and Its Relation to Photovoltaic Performance. *J. Phys. Chem. Lett.* **5**, 1035–1039 (2014).
32. A. Sadhanala *et al.*, Preparation of Single-Phase Films of CH₃NH₃Pb(I_{1-x}Br_x)₃ with Sharp Optical Band Edges. *J. Phys. Chem. Lett.* **5**, 2501–5 (2014).
33. R. L. Milot, G. E. Eperon, H. J. Snaith, M. B. Johnston, L. M. Herz, *Adv. Funct. Mater.*, in press, doi:10.1002/adfm.201502340.
34. W. Tress *et al.*, *Adv. Energy Mater.*, in press, doi:10.1002/aenm.201400812.
35. H. J. Snaith, Estimating the Maximum Attainable Efficiency in Dye-Sensitized Solar Cells. *Adv. Funct. Mater.* **20**, 13–19 (2010).
36. U. Rau, Reciprocity relation between photovoltaic quantum efficiency and electroluminescent emission of solar cells. *Phys. Rev. B.* **76**, 085303 (2007).
37. L. Mazzarella *et al.*, p-type microcrystalline silicon oxide emitter for silicon heterojunction solar cells allowing current densities above 40 mA/cm². *Appl. Phys. Lett.* **106**, 023902 (2015).
38. S.-M. Yong, N. Tsvetkov, L. Larina, B. T. Ahn, D. K. Kim, Ultrathin SnO₂ layer for efficient carrier collection in dye-sensitized solar cells. *Thin Solid Films.* **556**, 503–508 (2014).
39. K. Wojciechowski *et al.*, C60 as an Efficient n-Type Compact Layer in Perovskite Solar Cells. *J. Phys. Chem. Lett.* **6**, 2399–405 (2015).
40. K. Wojciechowski *et al.*, Heterojunction Modification for Highly Efficient Organic–Inorganic Perovskite Solar Cells. *ACS Nano.* **8**, 12701–12709 (2014).
41. I. Borriello, G. Cantele, D. Ninno, Ab initio investigation of hybrid organic-inorganic perovskites based on tin halides. *Phys. Rev. B.* **77**, 235214 (2008).
42. M. R. Filip, G. E. Eperon, H. J. Snaith, F. Giustino, Steric engineering of metal-halide perovskites with tunable optical band gaps. *Nat. Commun.* **5**, 5757 (2014).
43. J. H. Noh, S. H. Im, J. H. Heo, T. N. Mandal, S. Il Seok, Chemical management for colorful, efficient, and stable inorganic-organic hybrid nanostructured solar cells. *Nano Lett.* **13**, 1764–9 (2013).
44. U. Rau, Reciprocity relation between photovoltaic quantum efficiency and electroluminescent emission of solar cells. *Phys. Rev. B.* **76**, 085303 (2007).

Acknowledgments: This project was part funded by EPSRC through the Supergen Solar Energy Hub SuperSolar (EP/M024881/1) and (EP/M014797/1) the ERC through the Stg-2011 HYPER and the US Office of Naval Research (ONR). MH is funded by Oxford PV. WR is supported by the Hans-Boeckler-Foundation. We thank our colleagues from CREST Photovoltaic Measurement and Testing Laboratory, Loughborough University for their contributions to the measurements of the semi-transparent devices. We also thank K. Jacob & M. Wittig (HZB, Inst. Silicon Photovoltaics), L. Mazzarella & S. Kirner (HZB, Inst. PVcomB) for their contributions to fabricating the SHJ cell. The University of Oxford has filed a patent related to this work

Author Contributions: The project was designed and conceptualized by DM and HJS. DM performed experiments, analyzed data and wrote the paper. GS fabricated and measured devices with

semi-transparent electrodes. WR characterize the material using THz spectroscopy. GE helped with the experimental work and provided technical feedback on the writing of the paper. MS provided input and technical direction on the FA/Cs cation mixture. MH performed simulations for the optical modeling and calculated the maximum achievable V_{OC} . AH analysed XRD data. NS provided input on the preparation of thin films using chemical bath depositions. LK and BR fabricated the SHJ cells. MJ performed and analysed EQE measurements. LH supervised and analysed the THz spectroscopy measurements. HJS supervised the overall conception and design of this project.